

Fabrication of Field-Effect Transistors from Hexathiapentacene Single-Crystal Nanowires

Alejandro L. Briseno,^{*,†} Stefan C. B. Mannsfeld,[‡] Xianmao Lu,[†] Yujie Xiong,[†]
Samson A. Jenekhe,^{†,§} Zhenan Bao,^{*,‡} and Younan Xia^{*,†}

*Department of Chemistry, University of Washington, Seattle, Washington 98195,
Department of Chemical Engineering, Stanford University, Stanford, California 94305,
Department of Chemical Engineering, University of Washington,
Seattle, Washington 98195*

Received November 19, 2006; Revised Manuscript Received January 23, 2007

ABSTRACT

This paper describes a simple, solution-phase route to the synthesis of bulk quantities of hexathiapentacene (HTP) single-crystal nanowires. These nanowires have also been successfully incorporated as the semiconducting material in field-effect transistors (FETs). For devices based on single nanowires, the carrier mobilities and current on/off ratios could be as high as 0.27 cm²/Vs and >10³, respectively. For transistors fabricated from a network of nanowires, the mobilities and current on/off ratios could reach 0.057 cm²/Vs and >10⁴, respectively. We have further demonstrated the use of nanowire networks in fabricating transistors on mechanically flexible substrates. Preliminary results show that these devices could withstand mechanical strain and still remain functional. The results from this study demonstrate the potential of utilizing solution-dispersible, nanostructured organic materials for use in low-cost, flexible electronic applications.

Organic semiconductor nanostructures are potential next-generation materials for displays, integrated circuits, solar cells, memory elements, and actuators.¹ The advances in molecular design and synthesis has made it possible to tune the molecular structures and properties of organic semiconductors to meet the technological requirements for fabricating practical devices. Studies on aromatic molecules have shown that self-assembly through strong π - π interactions can lead to the formation of one-dimensional (1D) nanostructures preferred for field-effect transistors.²⁻⁴ Examples of self-assembled nanostructures include (but are not limited to) nanofibers, nanowires, and nanoribbons synthesized from hexabenzocoronene derivatives,^{2,5} perylene tetracarboxylic diimide derivatives,^{6,7} macrocyclic aromatic molecules,⁸ C₆₀,⁹ and metal phthalocyanines.^{3,10} One-dimensional nanostructures predominantly self-assemble along the π - π stacking direction,⁷ which is believed to favor a high charge-carrier mobility as a result of the strong intermolecular coupling between the packed molecules.¹¹ It has recently been shown that π -stacking in oligoacene derivatives can generate high carrier mobilities in transistor devices.^{12,13} Among the oligoacenes,¹⁴ pentacene¹⁵ and its derivatives^{13,16} have thus

far exhibited the best-reported device performance. Despite these promising results, there are very few reports¹⁷ on 1D nanostructures (e.g., nanowires) synthesized from oligoacenes, let alone pentacene derivatives. A possible explanation for this slow development is the relative scarcity of π -stacking pentacene derivatives.^{13,16,18}

One of the greatest challenges for organic thin-film transistors is to achieve an ultimate control of both film morphology and degree of crystallinity.¹⁹ Even the best-performing organic semiconductors inevitably contain molecular disorder and grain boundaries, which effectively reduces the mobility of the material.²⁰ Organic single crystals, on the other hand, are known to have superior performance²¹ as they are largely free of grain boundaries or molecular disorder. However, their fragility and brittleness makes it very difficult to work with and reports of fabricating devices from solution-processable single crystals are somewhat unusual.^{22,23} Solution deposition offers a cost-effective method for fabricating large-area electronic components from organic materials. While solution-deposition techniques have been reported with some level of success, there are still unresolved issues in controlling the crystal packing and film-forming properties. Therefore, there is a growing need to explore organic single-crystal nanostructures as solution-processable materials, which are expected to have a profound impact on the future of molecular and flexible electronics.

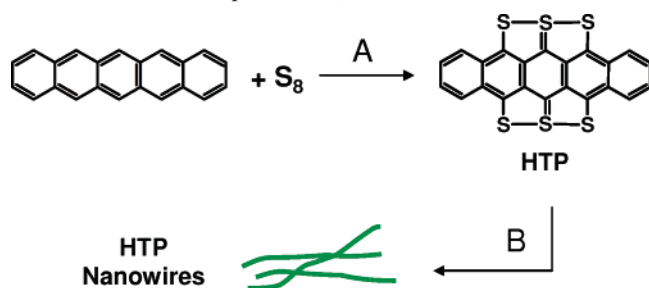
* Corresponding authors. E-mail: xia@chem.washington.edu (Y.X.); abriseno@u.washington.edu (A.L.B.); zbao@stanford.edu (Z.B.).

[†] Department of Chemistry, University of Washington.

[‡] Department of Chemical Engineering, Stanford University.

[§] Department of Chemical Engineering, University of Washington.

Scheme 1. Two Steps Involved in the Synthesis of Hexathiapentacene (HTP) Nanowires^a



^a (A) A mixture of pentacene and elemental sulfur are refluxed in trichlorobenzene for 3 h, and (B) HTP is recrystallized from an organic solvent with high boiling point such as benzonitrile, *o*-dichlorobenzene, or nitrobenzene. Addition of methanol can help reduce the size of resultant nanowires.

In this study, we demonstrate a solution-phase route to the facile synthesis of single-crystal nanowires of hexathiapentacene (HTP). We are interested in this molecule because it combines the elements of pentacene and peripherally rich sulfur atoms that favor π - π stacking.^{18,24} Our synthetic route produces bulk quantities of insoluble yet highly dispersible single-crystal HTP nanowires. We demonstrate that these nanowires are highly dispersible in a range of organic solvents to produce low-cost, large-area, mechanically flexible field-effect transistors with carrier mobilities as high as 0.27 cm²/Vs for single HTP nanowires and 0.056 cm²/Vs for devices containing a network of HTP nanowires. Thus far, organic nanostructures reported with the best performance for single-wire transistors were synthesized from CuPc and F₁₆CuPc via high-temperature (380–450 °C) physical vapor transport.³ Although the mobilities of HTP nanowires are only next to the values reported for these nanostructures, our solution-based synthesis allows for the production of HTP nanowires in large quantities as well as fabrication of solution-deposited devices over large areas.

We started the synthesis with the preparation of HTP from pentacene and elemental sulfur (Scheme 1).^{25,26} Because HTP is insoluble in nearly all organic solvents at room temperature, it can be readily dissolved in and recrystallized from organic solvents with high boiling points such as benzonitrile, nitrobenzene, and *o*-dichlorobenzene. The insolubility of HTP at room temperature serves as a key advantage for solution processability. In a typical process, 0.018 g of HTP powder was added into 15 mL of benzonitrile hosted in a 50 mL round-bottom flask and then refluxed under magnetic stirring. After the powder had been completely dissolved, both magnetic stirring and heating were turned off and the solution was slowly cooled down to induce crystallization. After several hours, HTP nanowires in a cottonlike state were observed floating in the solution. One could then collect the nanowires and transfer them into a poor solvent for HTP such as chloroform, methylene chloride, or ethanol. The nanowires settled out from the solution after several hours but could be easily redispersed by tapping the vial or simple agitation (Figure 1A,B). We note that there was a complete conversion of the dissolved HTP powder (from the as-

synthesized, polycrystalline sample) into the single-crystal nanowire form. Any excess HTP powder that was not dissolved during the refluxing process would remain as granular debris that quickly settled out from the solution once magnetic stirring was switched off. In this case, one could simply collect the suspended nanowires and disregard the debris that accumulated at the bottom of the reaction container. It is possible to control the widths of the nanowires from ~ 1 μm to ~ 150 nm by injecting small quantities of methanol into the recrystallization solution as the solution began to cool (see Supporting Information for precautions and details). Typical lengths of the nanowires ranged from several dozen μm to hundreds of μm , while the nanowire heights were in the range of 70 to 470 nm. Figure 1C shows SEM image of a network of HTP nanowires spun-cast onto a SiO₂/Si substrate from a 2 mg/mL HTP/chloroform solution at 800 rpm. Figure 1D shows an individual HTP nanowire of ~ 200 nm in diameter drop-cast on a SiO₂/Si substrate from a suspension in ethanol. Figure 1E shows a typical TEM image of a network of HTP nanowires. It is worth emphasizing that, unlike pentacene and other reported derivatives,^{14,16a} HTP nanowires are remarkably stable²⁶ in most organic solvents (including chlorinated solvents) and do not exhibit any bleaching even after being exposed to ambient conditions for more than 5 months. The chemical stability of HTP may be attributed to the relatively high ionization potential, which makes it more difficult to be oxidized as compared to pentacene (HOMO_{HTP} = -5.35 eV; HOMO_{pentacene} = -5.0 eV).^{16a,26} This particular attribute is very important for solution-processable organic semiconductors.

To correlate the observed morphology of HTP nanowires with the molecular crystal structure, we performed electron diffraction studies and crystallographic packing calculations. Figure 2A shows the TEM image of a single-crystal HTP nanowire, with the inset giving the corresponding electron diffraction pattern. The geometry of the TEM diffraction pattern and the measured spacings are in good agreement with the (001) plane of the vacuum-grown crystals.²⁶ The *d*-spacings of (100) and (010) were determined to be 3.84 and 14.5 Å, respectively, with an in-plane unit cell angle of 88°; the corresponding values from the vapor-grown crystal were 3.89 Å, 14.33 Å, and 84°. This suggests that the solution-grown and vapor-grown crystals possess (nearly) the same crystal structure and that, consequently, the long axis of the illustrated HTP nanowire corresponds to the [100] direction or the *a*-axis of the crystal unit cell. In the vacuum-grown crystal,²⁶ the HTP molecules exhibit the shortest stacking distance and thus the largest overlap of molecular orbitals along this direction. Figure 2B depicts the HTP single-crystal growth morphology as predicted using the attachment energy method.²⁷ For simplicity, the impact of solvation layer is neglected. In reality, the crystal in a solution should be covered by a solvation layer, which can lead to discrepancies between predicted and experimentally obtained crystal morphologies.²⁸ Furthermore, we assume the molecular structure of solution-grown HTP crystals to be identical to that of their vacuum-sublimation grown counterparts.²⁶ The attachment energies for various low-index crystal

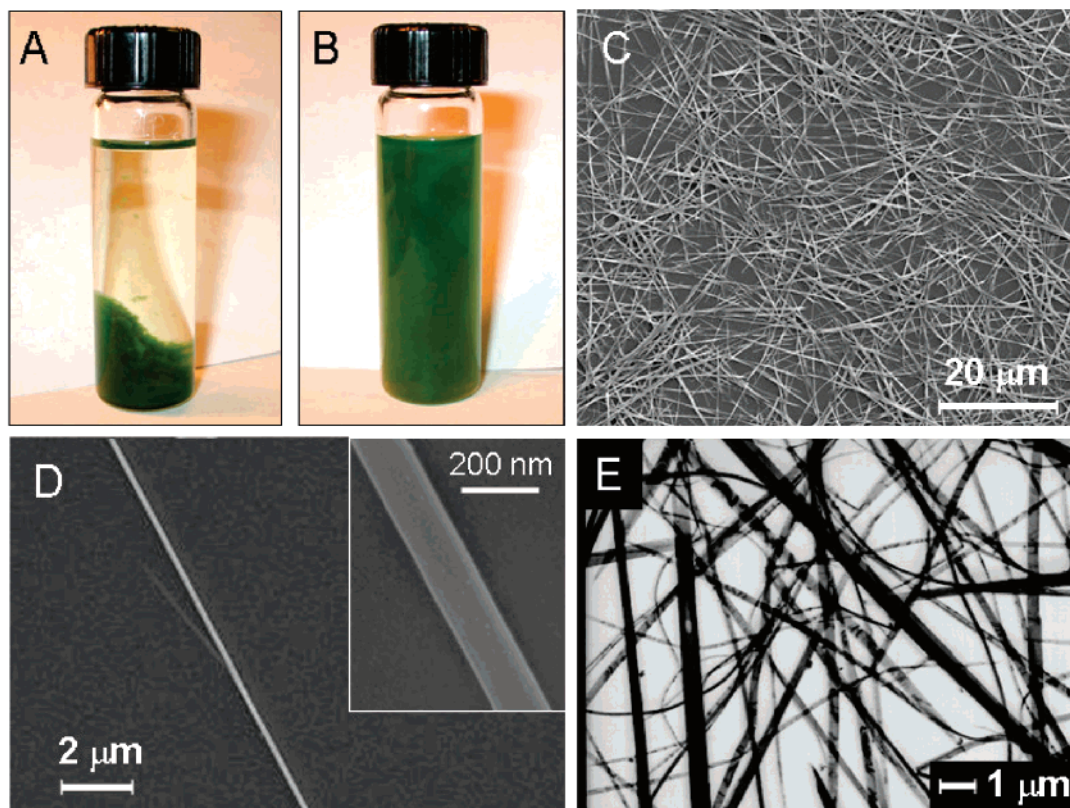


Figure 1. (A) Optical photograph showing the cottonlike state of HTP nanowires in chloroform, and (B) well-dispersed nanowires after agitating the vial. (C) SEM image of a network of HTP nanowires. (D) SEM image of an HTP nanowire with a width of <200 nm (see the inset for zoom-in). (E) TEM image of a network of HTP nanowires.

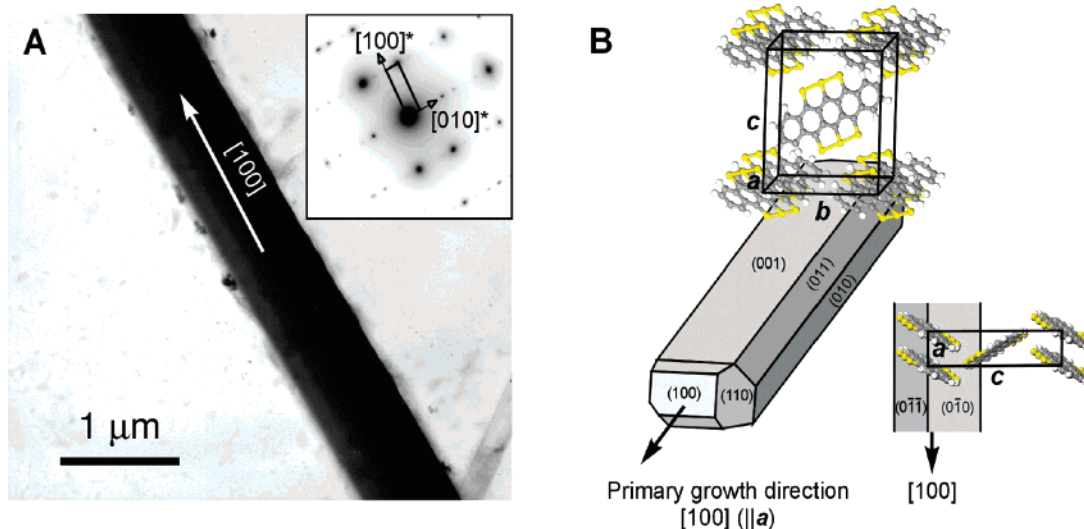


Figure 2. (A) TEM image of and electron diffraction pattern (inset) from a single-crystal HTP nanowire. The diffraction spots were recorded in the $[001]$ orientation, suggesting that the growth direction of the wire is $[100]$ (i.e., the unit cell axis a). (B) Theoretically predicted growth morphology of an HTP single crystal is based on the attachment energy method. The calculation indicates that the HTP crystal should be elongated in the $[100]$ direction along which the molecules exhibit a short stacking distance (3.8 \AA). This prediction is in agreement with the electron diffraction pattern even though the effect of solvation was neglected.

facets ($|h|, |k|, |l| \leq 1$) were computed using a Lennard-Jones potential function and the nonbonded interaction parameters from the universal force field.²⁹ By furthermore assuming that the relative growth rate of each crystal facet is proportional to the corresponding attachment energy,²⁷ the crystal shape was derived using the Wulff plot.³⁰

The HTP crystal is predicted to grow most rapidly along the $[100]$ direction (a -axis of the unit cell), which is in agreement with the electron diffraction data. Moreover, the calculation predicts the (001) facets to exhibit the largest surface area, i.e., the nanowire's basal plane should be a (001) facet.

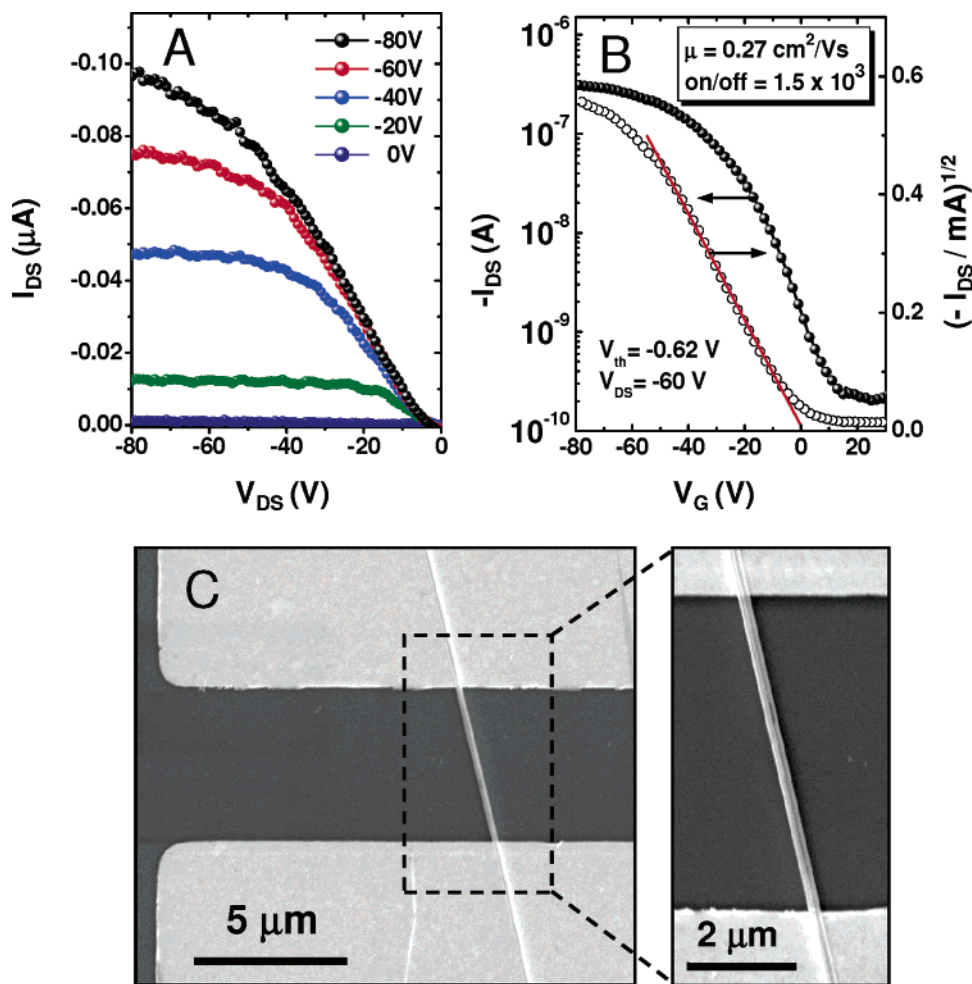


Figure 3. (A) Output and (B) transfer characteristics of an HTP single-nanowire transistor. The nanowire was cast from a dilute suspension in chloroform. (C) SEM image of a representative bottom-contact HTP nanowire device fabricated on a doped Si substrate that was covered by a SiO₂ dielectric layer of 300 nm thick. The inset shows a magnified view of the HTP nanowire bridging the source–drain gold electrodes. All measurements on HTP nanowire transistors were made under ambient conditions with a standard semiconductor probe station. Mobility values were calculated from individual HTP nanowires (see Figure S3C, Supporting Information).

Panels A and B of Figure 3 show the output and transfer properties of a single-wire device, exhibiting p-type characteristics with an estimated hole mobility of $\sim 0.27 \text{ cm}^2/\text{Vs}$ in the saturation region.³¹ Figure 3C shows a representative SEM image of a Cr/Au bottom-contact device constructed from a single HTP nanowire. For mobility calculations, the W/L was defined as the width of the nanowire and the length across the source–drain electrodes (see Supporting Information). The average W/L of a nanowire on a transistor device was ~ 0.059 . The nanowire was drop-cast across the source and drain electrodes from a dilute suspension of HTP nanowires in chloroform. Devices were annealed at $\sim 150 \text{ }^\circ\text{C}$ for 10 min and then placed in a vacuum oven at $60 \text{ }^\circ\text{C}$ overnight to ensure any traces of solvent would be completely removed. While this particular device showed a current on/off ratio of $\sim 10^3$, we occasionally measured on/off ratios as high as 10^4 . From Figure 3A, it can be seen that the onset of each output curve clearly reveals evidence of contact resistance, and for simplicity in mobility calculations, we neglected these effects in the analysis. A threshold voltage of -0.62 V was calculated at $V_{\text{DS}} = -60 \text{ V}$. Such a low threshold voltage is seldom observed in polycrystalline thin-

film devices but more often observed in single-crystal devices.²¹ It is also important to note that the nanowire transistors occasionally cease to function after one scan if the applied voltage is too high. Device failure may be possibly due to a relatively large current density passing through the nanowire, resulting in damage to either the nanowire or contacts (both dielectric–semiconductor and the electrode–semiconductor contacts). For measurements on different devices, we obtained mobilities in the range of $\sim 10^{-2}$ – $0.27 \text{ cm}^2/\text{Vs}$. This wide range of variation can be partly attributed to: (i) difference in contact quality at the dielectric–semiconductor and/or metal–semiconductor interface and (ii) solvent impurities and/or microscopic debris trapped at the dielectric–semiconductor interface. Nevertheless, an average value of $0.11 \pm 0.08 \text{ cm}^2/\text{Vs}$ was obtained from eight devices for saturation regime mobility. These characteristics are comparable to other thin-film transistors reported in literature^{15,16} and similar to recent reports of crystalline nanowire devices.^{2,3}

It is worth emphasizing that the highest mobility reported for single-crystal HTP nanowire transistors is over six times greater than that of vapor-deposited HTP thin-film transis-

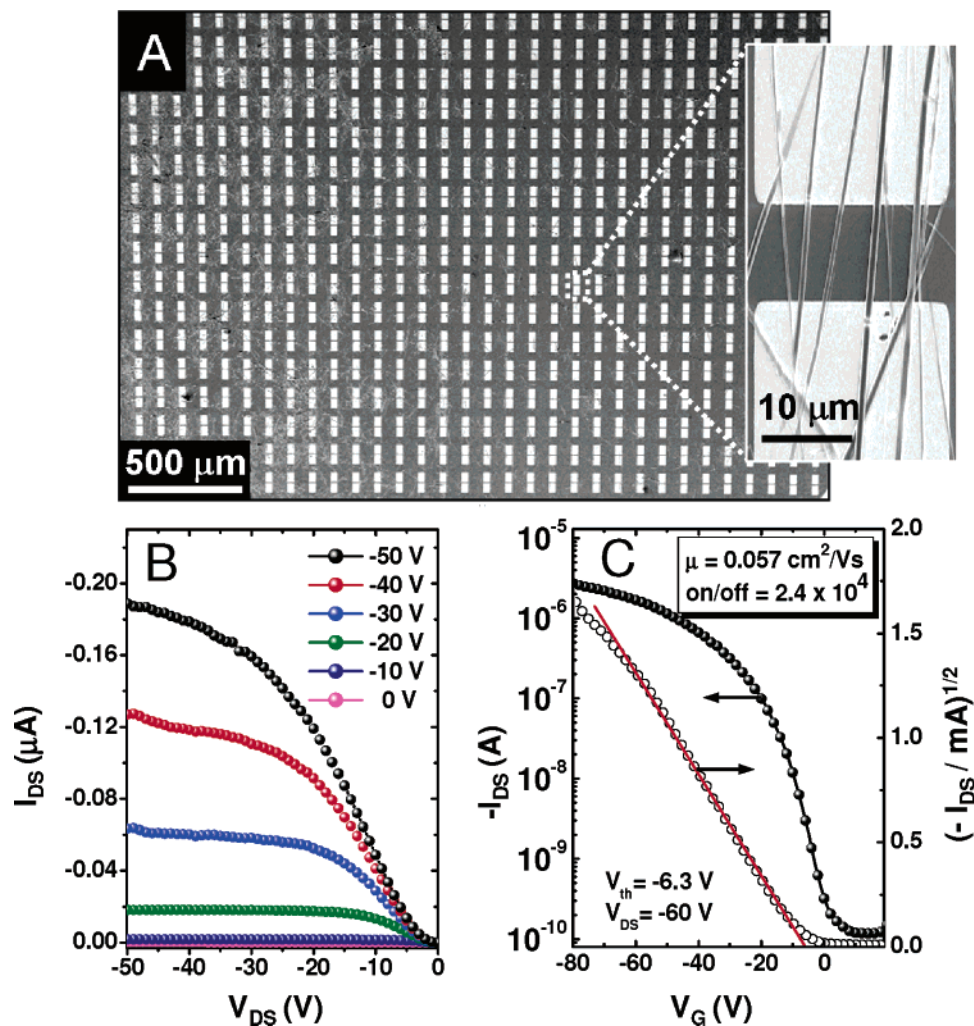


Figure 4. (A) SEM image of a large-area array of bottom-contact devices containing HTP nanowire networks cast from a 2 mg/mL suspension in chloroform. Inset shows a zoom-in of a device showing the nanowire network bridging the source and drain electrodes. Note that the nanowires overlap and stack across the channel. It is presumed that the disorder of nanowires across the channel is responsible for the lower mobility as compared with the single nanowire transistor. (B) Output and (C) transfer characteristics of an HTP network device. The electrical characteristics correspond to our best-performing network device.

tors.²⁶ In a recent report by Briseno et al.,²⁶ a mobility of $0.04 \text{ cm}^2/\text{Vs}$ and a current on/off ratio $> 10^6$ were demonstrated for HTP thin-film transistors. The higher mobility of the nanowire transistors compared to vapor-deposited thin-film transistors can be attributed to the high level of structural perfection of the single-crystal HTP nanowires in addition to the fact that they are essentially free of grain boundaries or monomolecular growth steps,^{21d,32} as evidenced from AFM surface measurements conducted on individual nanowires. Furthermore, it is not uncommon for mobility to be higher in single-crystals versus the thin-film form of a semiconductor material.^{12,33} The relatively large current on/off ratios for the HTP thin-film devices²⁶ can be ascribed to the OTS surface treatment, which is known to increase the current modulation in organic thin-film devices.^{15,16} In addition, thin-film transistors tend to have larger current on/off ratios over single-crystal devices.^{3b} In this study, we did not carry out any surface treatment on our devices.

A real-world challenge in addressing the manufacturing goals for flexible electronics and displays is the ability to fabricate and process organic transistors in a facile and low-

cost manner, over large areas, and on mechanically flexible substrates. With this objective in mind, we set about to fabricate arrays of transistors over large areas by employing the solution-processable feature of HTP nanowires. Figure 4A illustrates an array of source–drain electrodes covered by a network of HTP nanowires that were drop-cast from a suspension (2 mg/mL) of HTP nanowires in chloroform. Prior to solution-casting, the substrate was exposed to O_2 plasma for ~ 10 s in order to improve substrate wettability. The substrate was tilted at a 45° angle to enable the solution-borne HTP nanowires to trickle down the device to promote the alignment of the nanowires across the paired electrodes. It is worth noting that this provisional method of aligning nanowires is not entirely successful, as we often observed random networks that consisted of nanowires overlapping one another. Further optimization of nanowire alignment and patterning is needed and will be reported in due course. The inset in Figure 4A shows a network of wires bridging the source and drain electrodes of a typical HTP network transistor. Panels B and C of Figure 4 show the electrical characteristics of a network HTP transistor, exhibiting a hole

mobility of $0.057 \text{ cm}^2/\text{Vs}$ and a current on/off ratio of 2.4×10^4 . It is evident that this device also shows contact-limited behavior as indicated by the onset of the gate-modulated output curves. Nevertheless, the device still displays excellent gate modulation and current saturation. The lower mobility of the network transistor devices compared to the single-wire devices (4–5-fold difference in mobility) can be explained from the aforementioned description of crossing and overlapping nanowires across the source and drain electrodes. Random crossing and/or overlap of the network nanowires is reminiscent of grain boundaries in thin-film transistors, and it is no surprise that the average mobility ($0.042 \pm 0.015 \text{ cm}^2/\text{Vs}$) of the network devices is effectively reduced and quite similar to that of vapor-deposited HTP thin-film devices.²⁶

We fabricated the HTP nanowire transistors on mechanically flexible substrates to evaluate their potential for future applications in flexible electronics. Our approach to measuring the devices on plastic substrates is similar to the one described in recent reports.^{21a,32} Briefly, a shadow mask was used to evaporate Cr/Au source–drain electrodes for bottom-contact devices. Poly(vinylphenol) was utilized as the polymer dielectric layer, while gold or ITO-coated poly(ethyleneterephthalate) (PET) served as the gate electrode. To demonstrate the facile processability of the solution-dispersible nanowires, we spray-coated the material from a suspension (0.1 mg/mL) of HTP nanowires in a mixture of chloroform/ethanol (1:1). The spray-coating method allows one to control the density of nanowires across source–drain electrodes. Figure 5A shows the transfer characteristics of an HTP nanowire network device on a flexible substrate. A mobility of $0.032 \text{ cm}^2/\text{Vs}$, a current on/off ratio of $\sim 10^3$, and a threshold voltage of -8 V were obtained from a flexible device similar to that pictured in Figure 5B. Again, we speculate that the decrease in mobility compared to a single-wire transistor is due to the crossing and overlap of nanowires (see the inset in Figure 5B). Because it is difficult to estimate the active area of the nanowires, our mobilities reported here may very well be underestimated. The average mobility extracted from our HTP-network flexible devices is $0.017 \pm 0.01 \text{ cm}^2/\text{Vs}$.

We also fabricated single-nanowire transistors on flexible substrates to determine if the performance is similar to the devices fabricated on conventional Si/SiO₂ substrates. The highest mobility attained for such a device yielded a mobility of $0.19 \text{ cm}^2/\text{Vs}$ and a current on/off ratio of $> 10^3$ (see Supporting Information). The average mobility over six devices was $0.08 \pm 0.06 \text{ cm}^2/\text{Vs}$. This mobility is consistent with the performance of single-nanowire devices fabricated on rigid Si/SiO₂ substrates. Having demonstrated that HTP nanowire transistors successfully function on plastic, we then investigated the mechanical flexibility of HTP nanowires by conducting basic experiments to determine the effects of mechanical strain³⁴ on the performance of such a device. Hu et al. nicely demonstrated that CuPc/F₁₆CuPC nanoribbons possessed excellent flexibility.³ However, they did not report the effects of mechanical deformation on device performance. It was also recently demonstrated that organic single-crystal

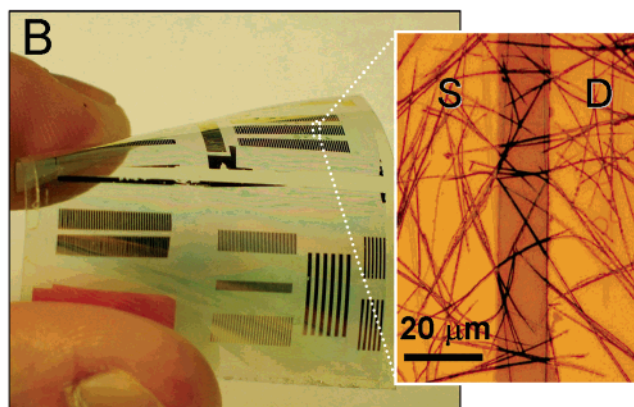
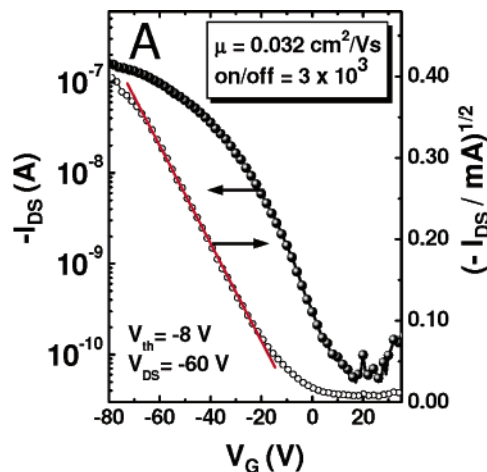


Figure 5. (A) Transfer characteristics for a device fabricated from a network of HTP nanowires on a flexible substrate (see Supporting Information). (B) Photograph of an array of bottom-contact nanowire network devices where the source–drain electrodes were deposited through a shadow mask. The inset shows a typical device covered with a network of HTP nanowires spray-coated from a suspension in a mixture of chloroform and ethanol (1:1). A $1.5 \mu\text{m}$ thick PVP dielectric layer was used for these devices, and its capacitance was $1.9 \text{ nF}/\text{cm}^2$.³²

transistors could achieve mechanical flexibility^{21a} by employing nanometer-thin rubrene single crystals.³² Apart from these studies, little is known on the mechanical properties of organic single crystals, and it is therefore deemed an important area of investigation. We conducted basic strain experiments³² on single nanowire devices only rather than on network nanowire devices. This was done in order to exclusively determine the performance of a nanostructured single crystal on a strained substrate; a network device would likely introduce inconclusive results as the devices contain overlapping nanowires. We first examined the flexibility of the nanowires by applying a tensile (outward bending) and compressive strain (inward bending) to the device by attaching it around an 18 mm diameter (radius curvature = 9 mm) glass cylinder and ensuring the device securely conformed to the cylindrical surface. All experiments were conducted on substrates bent across the channel length (L). The devices were first measured in the planar geometry mode followed by compressive strain, tensile strain, and finally back to the original planar geometry. The devices were held in the mechanically strained geometry for at least 2 h prior

to electrical measurements then allowed to rest for 1 h between successive experiments. We found no significant change in mobility from before, during, or after the applied strains. This trend has been routinely observed in at least six separate devices, with the only difference being in the effective mobility among the devices. Figure S2 in the Supporting Information shows the (I_{DS}) transfer overlays of a single-wire device subjected to various mechanical deformation geometries. Suo et al. determined that flexible Kapton substrates thinner than 300 μm become “compliant” and can significantly take up mechanical stress, thereby reducing the strain and prevent mechanical failure of the semiconductor.³⁴ Our conclusion from these preliminary experiments is that the performance of mechanically flexible nanowires are not significantly affected by the strenuous bending inflicted upon our devices.

In summary, this study introduces one of the first examples of a pentacene derivative, hexathiapentacene, which forms bulk quantities of single-crystal nanowires in a simple solution-phase synthesis. We demonstrated the solution processability of HTP nanowires by fabricating single-nanowire field-effect transistors and large-area arrays of transistors containing networks of nanowires. We further investigated the mechanical flexibility of the single-crystal nanowire transistors by demonstrating the effects of mechanical strain on the performance of our devices fabricated on flexible substrates. We discovered that single-nanowire devices have no significant loss in performance even after applying strenuous bending to the flexible substrate. These findings contribute to an area that is still in the very early stage of development, and we envision that further exploration of the mechanical properties of organic single-crystal nanowires will lead to their potential use in flexible electronics and displays.

Acknowledgment. A.L.B. acknowledges the Bell Labs Graduate Research Fellowship. S.C.B.M. acknowledges post-doc fellowship support by the Deutsche Forschungsgemeinschaft (DFG) grant MA 3342/1-1. Y.X. has been partially supported by the David and Lucile Packard Foundation and the GEMSEC, an NSF-supported MRSEC program. Z.B. acknowledges partial support from the Stanford MRSEC Center for Polymeric Interfaces and Macromolecular Assemblies (under NSF award DMR-0213618). We acknowledge Shuhong Liu and Colin Reese for kindly designing/fabricating some of the FET devices used in this study. We also thank Greg Golden and Vitaly Podzorov for valuable discussions and also the Nanotech User Facility (NTUF), a member of the National Nanotechnology Infrastructure Network (NNIN) funded by the NSF.

Supporting Information Available: Experimental procedures, details of device fabrication, and additional data. This material is available free of charge via the Internet at <http://pubs.acs.org>.

References

- (1) (a) Meijer, E. W.; Schenning, A. P. H. *J. Nature* **2002**, *419*, 353. (b) Hoeben, F. J. M.; Jonkheijm, P.; Meijer, E. W.; Schenning, A. P. H. *J. Chem. Rev.* **2005**, *105*, 1491.

- (2) Xiao, S.; Tang, J.; Beetz, T.; Guo, X.; Tremblay, N.; Siegrist, T.; Zhu, Y.; Steigerwald, M.; Nuckolls, C. *J. Am. Chem. Soc.* **2006**, *128*, 10700–10701.
- (3) (a) Tang, Q.; Li, H.; He, M.; Hu, W.; Liu, C.; Chen, K.; Wang, C.; Liu, Y.; Zhu, D. *Adv. Mater.* **2006**, *18*, 65–68. (b) Tang, Q.; Li, H.; Liu, Y.; Hu, W. *J. Am. Chem. Soc.* **2006**, *128*, 14634–14639. (c) Tang, Q.; Li, H.; Song, Y.; Xu, W.; Hu, W.; Jiang, L.; Liu, Y.; Wang, X.; Zhu, D. *Adv. Mater.* **2006**, *18*, 3010–3014.
- (4) Brisenno, A. L.; Roberts, M.; Ling, M.-M.; Moon, H.; Nemanick, E. J.; Bao, Z. *J. Am. Chem. Soc.* **2006**, *128*, 3880–3881.
- (5) Hill, J. P.; Jin, W.; Kosaka, A.; Fukushima, T.; Ichihara, H.; Shimomura, T.; Ito, K.; Hashizume, T.; Ishii, N.; Aida, T. *Science* **2004**, *304*, 1481–1483.
- (6) Yan, P.; Chowdhury, A.; Holman, M. W.; Adams, D. M. *J. Phys. Chem. B* **2005**, *109*, 724–730.
- (7) (a) Balakrishnan, K.; Datar, A.; Oitker, R.; Chen, H.; Zuo, J.; Zang, L. *J. Am. Chem. Soc.* **2005**, *127*, 10496–10497. (b) Datar, A.; Balakrishnan, K.; Yang, X.; Zuo, X.; Huang, J.; Oitker, R.; Yen, M.; Zhao, J.; Tiede, D. M.; Zang, L. *J. Phys. Chem. B* **2006**, *110*, 12327–12332.
- (8) Balakrishnan, K.; Datar, A.; Zhang, W.; Yang, X.; Naddo, T.; Huang, J.; Zuo, J.; Yen, M.; Moore, J. S.; Zang, L. *J. Am. Chem. Soc.* **2006**, *128*, 6576–6577.
- (9) Wang, L.; Liu, B.; Liu, D.; Yao, M.; Hou, Y.; Yu, S.; Cui, T.; Li, D.; Zou, G.; Iwasiewicz, A.; Sundqvist, B. *Adv. Mater.* **2006**, *18*, 1883–1888.
- (10) Tong, W. Y.; Djuricic, A. B.; Xie, M. H.; Ng, A. C. M.; Cheung, K. Y.; Chan, W. K.; Leung, Y. H.; Lin, H. W.; Gwo, S. *J. Phys. Chem. B* **2006**, *110*, 17406–17413.
- (11) (a) Curtis, M. D.; Cao, J.; Kampf, J. W. *J. Amer. Chem. Soc.* **2004**, *126*, 4318–4328 and references therein.
- (12) Moon, H.; Zeis, R.; Borkent, E.-J.; Besnard, C.; Lovinger, A. J.; Siegrist, T.; Kloc, Ch.; Bao, Z. *J. Am. Chem. Soc.* **2004**, *126*, 15322–15323.
- (13) Payne, M. M.; Parkin, S. R.; Anthony, J. E.; Kuo, C.-C.; Jackson, T. N. *J. Am. Chem. Soc.* **2005**, *127*, 4986–4987.
- (14) Bendikov, M.; Wudl, F.; Perepichka, D. F. *Chem. Rev.* **2004**, *104*, 4891–4945.
- (15) (a) Klauk, H.; Gundlach, D. J.; Nichols, J. A.; Jackson, T. N. *IEEE Trans. Electron. Devices* **1999**, *46*, 1259. (b) Klauk, H.; Halik, M.; Schieschang, V. Z.; Schmid, G.; Radilik, W.; Weber, W. *J. Appl. Phys.* **2002**, *92*, 5259. (c) Lin, Y.-Y.; Gundlach, D. J.; Nelson, S. F.; Jackson, T. N. *IEEE Trans. Electron. Devices* **1997**, *12*, 606–608.
- (16) (a) Meng, H.; Bendikov, M.; Mitchell, G.; Helgeson, R.; Wudl, F.; Bao, Z.; Siegrist, T.; Kloc, Ch.; Chen, C.-H. *Adv. Mater.* **2003**, *15*, 1090–1093. (b) Miao, Q.; Chi, X.; Xiao, S.; Zeis, R.; Lefenfeld, M.; Siegrist, T.; Steigerwald, M. L.; Nuckolls, C. *J. Am. Chem. Soc.* **2006**, *128*, 1340–1345. (c) Sheraw, C. D.; Jackson, T. N.; Eaton, D. L.; Anthony, J. E. *Adv. Mater.* **2003**, *15*, 2009–2011. (d) Miao, Q.; Lefenfeld, M.; Nguyen, T.-Q.; Siegrist, T.; Kloc, Ch.; Nuckolls, C. *Adv. Mater.* **2005**, *17*, 407–412.
- (17) Liu, H.; Li, Y.; Xiao, S.; Gan, H.; Jiu, T.; Li, H.; Jiang, L.; Zhu, D.; Yu, D.; Xiang, B.; Chen, Y. *J. Am. Chem. Soc.* **2003**, *125*, 10794–10795.
- (18) Kobayashi, K.; Shimaoka, R.; Kawahata, M.; Yamanaka, M.; Yamaguchi, K. *Org. Lett.* **2006**, *8*, 2385–2388.
- (19) McCulloch, I. *Nat. Mater.* **2004**, *4*, 583–584.
- (20) Dimitrakopoulos, C. D.; Malenfant, P. R. L. *Adv. Mater.* **2002**, *14*, 99.
- (21) (a) Brisenno, A. L.; Mannsfeld, S. C. B.; Ling, M.; Liu, S.; Tseng, R. J.; Reese, C.; Roberts, M.; Yang, Y.; Wudl, F.; Bao, Z. *Nature* **2006**, *444*, 913–917. (b) Sundar, V. C.; Zaumseil, J.; Podzorov, V.; Menard, E.; Willett, R. L.; Someya, T.; Gershenson, M. E.; Rogers, J. A. *Science* **2004**, *303*, 1644. (c) de Boer, R. W. I.; Gershenson, M. E.; Morpurgo, A. F.; Podzorov, V. *Phys. Status Solidi* **2004**, *201*, 1302. (d) Gershenson, M. E.; Podzorov, V.; Morpurgo, A. F. *Rev. Mod. Phys.* **2006**, *78*, 973–989.
- (22) Mas-Torrent, M.; Durkut, M.; Hadley, P.; Ribas, X.; Rovira, C. *J. Am. Chem. Soc.* **2004**, *126*, 984–985.
- (23) Gelinck, G. H.; Huitema, H. E. A.; van Veenendaal, E.; Cantatore, E.; Schrijnemakers, L.; van der Putten, J. B. P. H.; Geuns, T. C. T.; Beenhakkers, M.; Giesbers, J. B.; Huisman, B.-H.; Meijer, E. J.; Benito, E. M.; Touwslager, F. J.; Marsman, A. W.; van Rens, B. J. E.; de Leeuw, D. M. *Nat. Mater.* **2004**, *3*, 106.
- (24) Cho, D. M.; Parkin, S. R.; Watson, M. D. *Org. Lett.* **2005**, *7*, 1067–1068.
- (25) Goodings, E. P.; Mitchard, D. A.; Owen, G. *J. Chem. Soc., Perkin Trans. 1* **1972**, 1310–1314.

- (26) Briseno, A. L.; Miao, Q.; Ling, M.-M.; Reese, C.; Meng, H.; Bao, Z.; Wudl, F. *J. Am. Chem. Soc.* **2006**, *128*, 15576–15577.
- (27) Hartman, P.; Bennema, P. *J. Cryst. Growth* **1980**, *49*, 145–156.
- (28) Berkovitchyellin, Z. *J. Amer. Chem. Soc.* **1985**, *107*, 8239–8253.
- (29) Casewit, C. J.; Colwell, K. S.; Rappe, A. K. *J. Amer. Chem. Soc.* **1992**, *114*, 10035–10046.
- (30) Wulff, G. *Z. Kristallogr. Mineral.* **1901**, *34*, 449–530.
- (31) The field-effect mobility was calculated in the saturation region from the given equation, $I_{DS} = (W \cdot C \cdot \mu / 2 \cdot L) (V_G - V_T)^2$, where the capacitance, $C = 10 \text{ nF/cm}^2$ for 300 nm thick SiO₂ gate dielectric and V_T is the threshold voltage.
- (32) Briseno, A. L.; Tseng, R. J.; Ling, M.-M.; Falcao, E. H. L.; Yang, Y.; Wudl, F.; Bao, Z. *Adv. Mater.* **2006**, *18*, 2320–2324.
- (33) Briseno, A. L.; Tseng, R. J.; Ling, M.-M.; Falcao, E. H. L.; Meng, H.; Yang, Y.; Wudl, F.; Bao, Z. *Appl. Phys. Lett.* **2006**, *89*, 222111.
- (34) See Supporting Information for calculated strain equation given from Suo and coworkers: (a) Gleskova, H.; Wagner, S.; Suo, Z. *Appl. Phys. Lett.* **1999**, *75*, 3011–3013. (b) Suo, Z.; Ma, E. Y.; Gleskova, H.; Wagner, S. *Appl. Phys. Lett.* **1999**, *74*, 1177–1179.

NL0627036